Letter

Ghost Spectroscopy with Classical Thermal Light Emitted by a Superluminescent Diode

Patrick Janassek, Sébastien Blumenstein, and Wolfgang Elsäßer[*]

Institute of Applied Physics, Technische Universität Darmstadt, 64289 Darmstadt, Germany

We propose and realize the first classical ghost-imaging (GI) experiment in the frequency or wavelength domain, thus performing ghost spectroscopy using thermal light exhibiting photon bunching. The required wavelength correlations are provided by light emitted by spectrally broadband near-infrared amplified spontaneous emission of a semiconductor-based superluminescent diode. They are characterized by wavelength-resolved intensity cross-correlation measurements utilizing two-photon-absorption interferometry. Finally, a real-world spectroscopic application of this ghost spectroscopy with a classical light scheme is demonstrated in which an absorption band of trichloromethane (chloroform) at 1214 nm is reconstructed with a spectral resolution of 10 nm as a proof-of-principle experiment. This ghost-spectroscopy work fills the gap of a hitherto missing analogy between the spatial and the spectral domain in classical GI modalities, with the expectation of contributing towards a broader dissemination of correlated photon ghost modalities, hence paving the way towards more applications which exploit the favorable advantages.

Ghost imaging (GI) is an imaging technique exploiting spatial intensity correlations of light. A ghost image is obtained by correlating the detected intensities of two separated light beams. However, only one of them interacts with the object. Intriguingly, the detector which does not see the object provides the spatial resolution of the reconstructed image. This rather counterintuitive imaging modality was realized by utilizing both quantum light and thermal light sources. The transfer of the GI phenomenon from the spatial to the frequency or wavelength domain has already been achieved by using nonclassical light exploiting quantum frequency correlations of entangled photon pairs.

Ghost Imaging (GI) was first demonstrated in 1995 with entangled light from a parametric down-conversion source [1] and was therefore initially claimed to be a pure quantum effect. In 2002, a GI experiment with a thermal light source exhibiting classical intensity fluctuations was achieved [2], and many succeeding experiments have proven that GI cannot be considered a quantum effect only [3–5]. Since then, numerous GI developments have been reported [6] regarding new configurations with improved correlation protocols [7–9], new light sources [10–12], new detection techniques [13–15], and the exploration of potential application areas [16–19]. Also, the GI phenomenon has been carried beyond the optical range using x rays [20]. Even the particle regime has been entered using correlated atoms [21].

Concurrently, various ghost modalities have been developed which can be regarded as respective analogies (see Table I). Besides the GI phenomenon, which is based on

spatial correlations of light to form images, temporal GI has been realized to exploit temporal correlations of light where a temporal object is retrieved. For instance, a bit sequence is modulated onto the amplitude of intensity fluctuations and subsequently recorded by a detector with low bandwidth. Therefore, the time sequence is not resolved. However, the intensity of a highly temporally correlated reference beam is then recorded by a high-bandwidth detector. In fact, the cross-correlations between the two signals allow one to recover the time sequence. This temporal analog of GI has been realized with nonclassical light [22] and incoherent thermal-like light [23] as well as artificially randomized light by computational methods [24] (see Table I).

Another ghost modality—namely, ghost spectroscopy—has been developed that utilizes frequency quantum correlations of entangled photon pairs [25]. Specifically, twin photons from a spontaneous parametric down-conversion source are generated. Only the signal photons illuminate the sample and their totally transmitted light is registered by an integrating detector, whereas the idler photons are sent through a monochromator and subsequently recorded by a spectrally resolving detector. The frequency entanglement between the signal and idler photons leads to the reconstruction of the frequency-dependent absorption features of the sample when correlating the two detector signals as a function of the reference frequency. Similar spooky quantum spectroscopy methods have already demonstrated real-world applications such as the determination of refractive indices and the absorption of CO_2 gas [29]. For spectroscopy applications with low light illumination, an enhancement of the signal-to-noise performance had

[*]elsaesser@physik.tu-darmstadt.de

TABLE I.   Introductory overview of representative experimental research on ghost-imaging modalities. The table summarizes representative achievements on GI, ghost spectroscopy, and temporal GI through quantum, thermal, and computational light-source approaches.

Modality		Experimental demonstrations		
Terminology	Correlations	Twin photons	Thermal light	Computational
Ghost imaging (GI)	Spatial	[1]	[2–4]	[13]
Ghost spectroscopy	Spectral	[25]	x	Multiplex spectroscopy [26,27]
Temporal GI	Temporal	[28]	[22,23]	[24]

been achieved by multiplexing methods many years before the first GI experiment [26,27]. There, spatial masks (Hadamard masks) were utilized such as modern computational imaging methods apply them via programmable spatial light modulators (e.g., digital micromirror devices [30]); one can associate this method with computational ghost spectroscopy. Table I summarizes this brief overview of existing experimental realizations of GI analogies by enumerating representative references. From there, it becomes clear that, even today, no ghost-spectroscopy experiment with classical light has been realized using thermal light sources. One of the reasons for this missing demonstration might be the technical demands of high time resolution τ_{meas} ($\tau_{\mathrm{meas}} \ll \tau_c$) when intensity correlations of spectrally broadband light ($\tau_c = 1/\Delta\nu$) are measured. A secondary reason could be the difficulty in finding a practical light source that provides a broadband spectrum, as well as the required wavelength correlations in order to enable the ghost-spectroscopy modality.

In this Letter, we show experimentally that spectrally broadband light emitted by a quantum-dot superluminescent diode (SLD) indeed exhibits classical wavelength correlations reflected by second order wavelength-wavelength (λ-λ) correlations which rapidly decay with an increasing wavelength separation, thus giving high spectral resolution. This finding is then exploited to realize a proof-of-principle experiment in which an absorption feature of liquid chloroform is reconstructed by the ghost-spectroscopy modality. No spectral resolution is provided there by the beam which interacts with the fluid. Instead, the reference arm yields the spectral resolution. By cross-correlating the two intensities, a ghost spectrum is formed which reflects the absorption feature. These experiments demonstrate a hitherto missing analogy between the spatial and spectral domains in classical GI.

Superluminescent diodes are semiconductor-based optoelectronic emitters capable of emitting spectrally broadband light with several tens to hundreds of nanometers of spectral width in terms of wavelength, together with considerable output powers. Therefore, a broadband optical gain material is embedded inside a waveguide structure. To prevent a lasing operation, the facets are antireflection coated and slightly tilted with respect to the waveguide. The length of the waveguide, typically several millimeters, allows spontaneously emitted photons to be amplified significantly by so-called amplified spontaneous emission (ASE). Here, we apply SLDs based on a quantum-dot (QD) active medium consisting of inhomogeneously broadened InAs/(In, Ga)As dot-in-well layers. Figure 1 shows a schematic drawing of the experimental setup with the SLD on the bottom right side as the ghost-spectroscopy light source. The emitted light from the front facet is collimated and sent through an optical isolator to prevent optical feedback. Through a beam splitter, SLD light passes a spectroscopic sample and the totally transmitted light is coupled into a single-mode fiber (SMF). The reflected part from the beam splitter serves as the reference arm where the spectral selectivity is located. Here, variable interference filters with a full width at half maximum (FWHM) of approximately 10 nm are utilized, followed also by SMF coupling optics. Both fiber-coupled beams are superimposed by a fiber combiner forming an overall Mach-Zehnder–like interferometer (MZI) configuration. Finally, the light is focused onto the semiconductor photocathode of a photomultiplier (PMT). The two-photon-absorption (TPA) interferometry technique employed here goes back to the work of Boitier et al. [31], who demonstrated for the first time the photon-bunching effect for blackbody sources with multiple-terahertz-wide optical spectra. The nonlinear TPA process requires two photons to be absorbed within a time frame given by the Heisenberg uncertainty. Hence, an ultrafast intensity-intensity correlation detection $\langle I(t)I(t)\rangle$ is enabled. The implementation of a time delay τ in the MZI
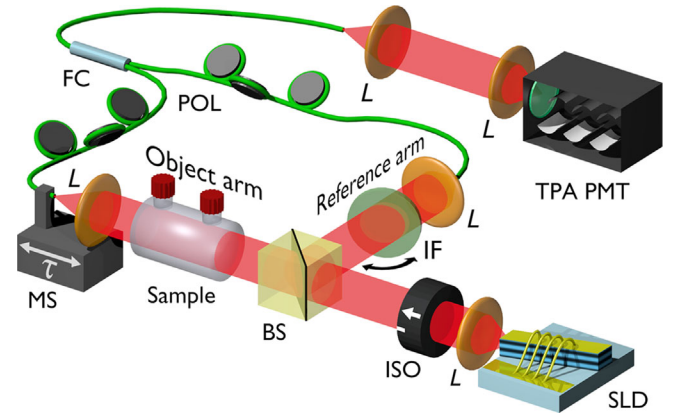

FIG. 1.   Schematic diagram of the ghost-spectroscopy experiment. The setup comprises the light source (SLD), collimating and focusing achromatic lenses (L), a two-stage optical isolator (ISO), a nonpolarizing beam splitter (BS), a tiltable interference filter (IF) in the reference arm followed by a fiber coupling unit, a sample within the object arm, again followed by a fiber coupling unit, a single-mode fiber-based combiner (FC), a motorized linear translation stage (MS), polarization-controlling elements (POL), and the PMT (Hamamatsu H7421-40) operated in TPA mode (TPA PMT), including a long-pass filter (Schott RG1000) that prevents visible light from entering the detector.

(see Fig. 1) enables intensity autocorrelation measurements $\langle I(t)I(t+\tau)\rangle$. The photomultiplier in use incorporates a (Ga,As)P photocathode which has been selected regarding the emitted wavelengths of the source in order to guarantee pure TPA detection. By reading out the photon counts from the detector output while varying the optical path of one interferometer arm using a high-precision motorized linear translation stage, a TPA interferogram $I_{\mathrm{TPA}}(\tau)$ is recorded,

$$\frac{I_{\mathrm{TPA}}(\tau)}{I_1 + I_2} = 1 + G^{(2)}(\tau) + \mathrm{Re}[F_2(\tau)\exp(-2i\omega_0\tau)]$$
$$+ 4\mathrm{Re}[F_1(\tau)\exp(-i\omega_0\tau)]. \quad (1)$$

In theory [31], three contributions arise: the non-normalized second-order autocorrelation function $G^{(2)}(\tau) = \langle I(t)I(t+\tau)\rangle$ and two fast oscillating terms $F_1(\tau)$ and $F_2(\tau)$ following the center angular frequency $\omega_0 = 2\pi\nu_0$ and the frequency duplication $2\omega_0$ of the emitted light, respectively. The latter results from the nonlinear absorption process. Additionally, the interferogram needs to be normalized to the mean photon count signals I_1 and I_2 of the individual interferometer arms. The normalized second-order correlation function is finally calculated as

$$g^{(2)}(\tau) = G^{(2)}(\tau)/G^{(2)}(\tau \gg \tau_c). \quad (2)$$

In the first place, the basic requirement for a ghost-spectroscopy modality is quantified, namely, the wavelength correlations of the light source. The SLD is operated at room temperature and the pump current is set to approximately 450 mA, well above the ASE threshold. Its emitted light exhibits a central wavelength of 1203 nm and a Gaussian-like distribution with a FWHM of 26 nm (see Fig. 2, the
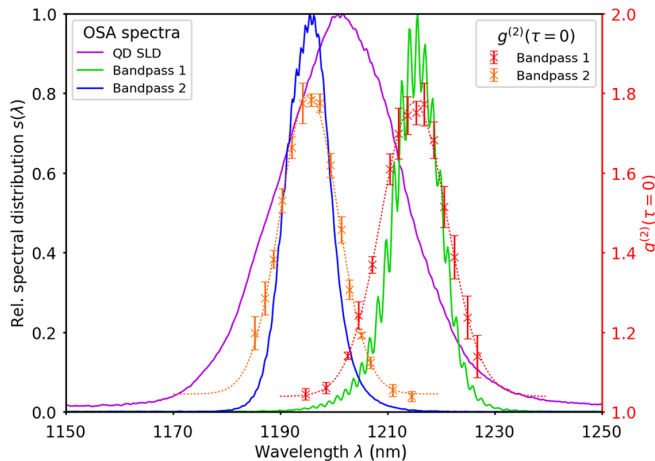

FIG. 2. Measured wavelength correlations of light emitted by the SLD. The full optical spectrum of the SLD (the magenta line, left scale) has been measured by a commercial optical spectrum analyzer (OSA, Advantest Q8384). Two representative—by interference filters—selected wavelength bands are also depicted (the green and blue lines, left scale). The second-order correlation results for the two bands are shown as red and orange crosses (right scale). The error bars correspond to the variance of a set of five measurements.

magenta line). The shape of the spectrum is due to single-state (ground-state) emission of the optically active QDs [32]. By selecting a wavelength band in one interferometer arm (Fig. 1, the object arm), utilizing a fixed interference filter and tilting successively another interference filter within the reference arm, the λ-λ intensity correlations

$$G^{(2)}(\tau, \lambda_{\mathrm{obj}}, \lambda_{\mathrm{ref}}) = \langle I_{\mathrm{ref}}(t, \lambda_{\mathrm{ref}})I_{\mathrm{obj}}(t+\tau, \lambda_{\mathrm{obj}})\rangle_t \quad (3)$$

are measured by the TPA detection technique. Figure 2 shows the spectra of two representative measurements, where the fixed bandpass windows are centered at 1215.5 ± 5.2 nm (bandpass 1, the green line) and at 1195.3 ± 4.8 nm (bandpass 2, the blue line). In both measurements, the mean wavelength of the corresponding reference filter ($\Delta\lambda_{\mathrm{FWHM}} \approx 10$ nm) is varied such that the object bandpass window is reasonably covered. The resulting $g^{(2)}(\tau = 0, \lambda_{\mathrm{obj}}, \lambda_{\mathrm{ref}})$ values are plotted in red and orange as a function of λ_{ref} in Fig. 2 as well. One can observe second-order correlation coefficients between $g^{(2)} \approx 1.05$ and $g^{(2)} \approx 1.80$. This nearly full-scale variation of the normalized wavelength correlation coefficient $g^{(2)}$ values from no correlation ($g^{(2)} \approx 1$) to a thermal photon-bunching behavior ($g^{(2)} \approx 2$) reveals a remarkable degree of wavelength-dependent intensity correlations of the emitted light from the SLD. A Gaussian fit to the $g^{(2)}(\lambda_{\mathrm{ref}})$ data traces accurately the experimental values which can be associated with a convolution of the Gaussian-shaped bandpass spectra. This is also the reason for the slight broadening of the wavelength correlation trajectories ($\mathrm{FWHM}_{\mathrm{BP1}} = 14.6$ nm and $\mathrm{FWHM}_{\mathrm{BP2}} = 12.7$ nm) with respect to the fixed bandpass windows. It coincides nicely with expected larger convolution widths $\Delta\lambda = \sqrt{2}\Delta\lambda_{\mathrm{FWHM}} = 14.2$ nm of the convolution of two Gaussian distributions assuming equal individual widths of $\Delta\lambda_{\mathrm{FWHM}} \approx 10$ nm.

From the temporal analysis of the full interferograms as a function a wavelength difference, we can also quantify the decrease of the central $g^{(2)}$ values with increasing frequency separation (as depicted in Fig. 2). A Gaussian fit to the $g^{(2)}(\tau)$ curves as a function of delay time τ yields typical FWHM values of the characteristic time of 280 fs with no significant wavelength dependence. This first experiment already represents a fundamental result, namely, the experimental verification of wavelength correlations of spectrally broadband ASE from a semiconductor light source, here in terms of a QD SLD. The spectral cross-correlation measurements of light with approximately 10-nm spectral widths, which result in ultrashort correlation time scales of approximately 0.4 ps, can be resolved only by TPA interferometry. The physical origin of these wavelength correlations might be based on the inhomogeneously broadened quantum-dot emitters of the active SLD medium.

The results of Fig. 2 suggest that photons generated by equally sized quantum dots, and hence of equal energy (wavelength), are more correlated in the amplification

process of ASE than those originating from quantum dots of differing sizes. To pursue these λ-λ correlation results towards a first ghost-spectroscopy experiment, an actual spectroscopic application exploiting these wavelength correlations is presented next.

Specifically, an absorption band of trichloromethane (chloroform, $CHCl_3$) at 1214 nm is analyzed by the ghost-spectroscopy modality. To match the wavelength range of the absorption feature, a chirped $InAs/(In, Ga)As$ QD SLD emitting at 1228 nm with a FWHM of 33 nm is chosen. Figure 3 (the purple line) shows a representative optical spectrum of the SLD in operation covering the spectral interval of 1190–1260 nm. Additionally, a standard transmission spectrum of the cuvette containing liquid chloroform with an absorption length of 100 mm is recorded (the green line). Now, for a proof-of-principle ghost-spectroscopy experiment, the scheme of Fig. 1 is applied. The chloroform cuvette is placed inside the object beam path. The totally transmitted light is coupled to the SMF, and thus no spectral information can be obtained. The complementary beam path—namely, the spectrally resolving reference arm—does not interact with the sample. Four variable interference filters with a bandpass width of 10 nm that differ in central wavelength are subsequently inserted into the reference arm to cover the full spectral emission range of the SLD. In accordance with the analogy between GI and GS, we define and exploit a ghost-spectroscopy (GS) detection protocol for our experimental GS setup depicted in Fig. 1 by using the GI terminology and replacing the spatial coordinate x by the spectral variable λ, such that the intensity cross-correlation coefficients as a function of reference-arm wavelength

$$g^{(2)}(\tau = 0, \lambda_{\text{ref}}) = \frac{\langle I_{\text{ref}}(t, \lambda_{\text{ref}}) I_b(t) \rangle_t}{\langle I_{\text{ref}}(t, \lambda_{\text{ref}}) \rangle_t \langle I_{\text{obj}}(t + \tau, \lambda_{\text{obj}}) \rangle_t} \quad (4)$$

now represent the ghost spectrum and are determined by TPA detection. We note that this new detection protocol in the spectral domain is based on the classical definition of the second-order Glauber correlation function in the spatial domain which represents the most basic GI signal detection [33]. In the sense of a spectrally integrating bucket detection scheme, such as for the ghost-imaging modality, the fiber-coupled intensity of the sample path can be expressed by

$$I_b(t) = \int I_{\text{obj}}(t, \lambda_{\text{obj}}) T_{CHCl_3}(\lambda_{\text{obj}}) d\lambda_{\text{obj}}, \quad (5)$$

where $I_{\text{obj}}(t, \lambda_{\text{obj}})$ corresponds to the intensity distribution of the SLD light entering the cuvette and $T_{CHCl_3}(\lambda_{\text{obj}})$ represents the spectral chloroform transmission.

Figure 3 (the red data) depicts the correlation coefficient data $g^{(2)}(\tau = 0, \lambda_{\text{ref}})$, i.e., the ghost spectrum as a function of the spectral position of the interference filters in the reference arm. Its mean central wavelengths are calibrated using OSA measurements. The trajectory of the experimental values reflects two key features: (i) $g^{(2)}$ values follow the overall SLD spectrum. The maximum value of $g^{(2)} = 1.27$ corresponds to the peak of the spectral distribution of the SLD. Also, the decreasing distribution wings are reflected by reducing correlation values down to $g^{(2)} = 1.05$. (ii) Most importantly, the absorption band at 1214 nm is directly reflected by $g^{(2)}(\tau = 0, \lambda_{\text{ref}})$, i.e., the measured ghost spectrum.

The overall reduced correlation values in comparison with the wavelength correlation measurement (Fig. 2) are due to the fact that the object arm contains a wide range of uncorrelated frequencies, in full analogy to the bucket detection in GI, where multiple uncorrelated spatial modes reduce the correlation signal contrast [34,35]. The absorption bandwidth of 11.3 nm [FWHM from a Voigt fit to the OSA measured data (the green data in Fig. 3)] centered at 1214.4 nm is well reproduced by the ghost spectrum of the chloroform sample, where a Gaussian fit to the relevant $g^{(2)}(\tau = 0, \lambda_{\text{ref}})$ data yields a FWHM of 10.7 nm centered at 1215.1 nm.

These findings coincide well with the reference data of chloroform, where the absorption band is attributed to overtones of the C-H–group stretch mode and to combination vibrations ($\lambda_c = 1213.9$ nm, $\Delta\lambda_{\text{FHWM}} = 8.7$ nm) [36]. From the Gaussian amplitude of the $g^{(2)}$ fit, one can deduce a correlation reduction of $\Delta g^{(2)} \approx 0.08$ as the ghost-absorption strength resulting from a chloroform path length of 100 mm. Slight artifacts such as the steplike behavior at 1233 and 1242 nm are attributed to the exchange of the interference filters. Still, the ghost spectrum successfully reconstructs the absorption band of chloroform at 1214 nm, which represents the first ghost-spectroscopy demonstration with thermal intensity correlations.
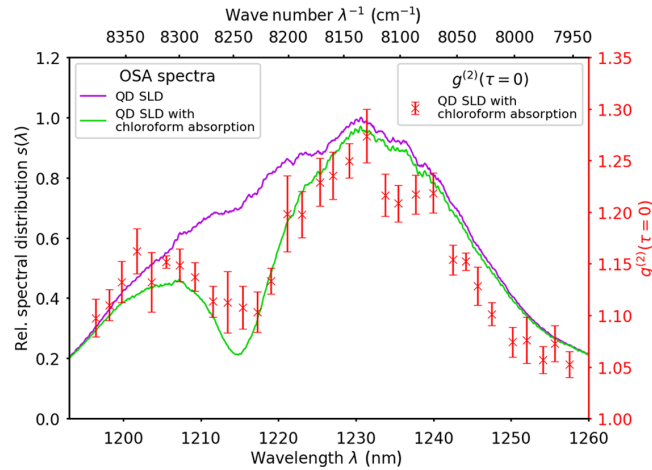

FIG. 3.   Experimental results of the ghost-absorption-spectroscopy experiment. The data points (the red crosses, right scale) represent the second-order λ-λ correlation values [Eq. (4)]—thus the ghost spectrum measured in Fig. 1—whereas the solid lines (left scale) depict an OSA measurement of the pure QD-SLD emission spectrum (magenta) and of the QD SLD with the filled liquid chloroform cuvette (the green line). The bottom scale is in wavelength, whereas the top scale exhibits a wave number scale.

In upcoming work, we plan to improve the spectroscopy performance of the proposed scheme, such as the spectral resolution. The coarse spectral resolution of 10 nm is utilized solely for demonstration purposes. Modeling is necessary to investigate the connection between the $g^{(2)}$ amplitudes and specific input spectra for the TPA detection in order to relate the ghost spectrum to an absorption strength.

In this Letter, we describe a classical GI experiment in the wavelength domain, thus performing ghost spectroscopy using thermal light exhibiting photon bunching. The prerequisite of wavelength-dependent intensity correlations is realized by spectrally broadband amplified spontaneous emission from superluminescent diodes. Only by exploiting TPA interferometry these broadband intensity correlations can be resolved on subpicosecond correlation time scales. By demonstrating the phenomenon within a real-world absorption spectroscopy experiment at liquid chloroform, its applicability to ghost spectroscopy is approved. This work fills a gap of experimental demonstrations of ghost-imaging modalities (see Table I). Whereas spatial GI and temporal GI have been achieved with nonclassical photon sources, with thermal light as well as by computational methods, ghost spectroscopy has still not yet been realized with thermal light sources.

ACKNOWLEDGMENTS

[1] T. B. Pittman, Y. H. Shih, D. V. Strekalov, and A. V. Sergienko, Optical imaging by means of two-photon quantum entanglement, Phys. Rev. A 52, R3429 (1995).

[2] R. S. Bennink, S. J. Bentley, and R. W. Boyd, "Two-Photon" Coincidence Imaging with a Classical Source, Phys. Rev. Lett. 89, 113601 (2002).

[3] F. Ferri, D. Magatti, A. Gatti, M. Bache, E. Brambilla, and L. A. Lugiato, High-Resolution Ghost Image and Ghost Diffraction Experiments with Thermal Light, Phys. Rev. Lett. 94, 183602 (2005).

[4] A. Valencia, G. Scarcelli, M. D'Angelo, and Y. Shih, Two-Photon Imaging with Thermal Light, Phys. Rev. Lett. 94, 063601 (2005).

[5] D. Zhang, Y.-H. Zhai, L.-A. Wu, and X.-H. Chen, Correlated two-photon imaging with true thermal light, Opt. Lett. 30, 2354 (2005).

[6] B. I. Erkmen and J. H. Shapiro, Ghost imaging: From quantum to classical to computational, Adv. Opt. Photonics 2, 405 (2010).

[7] K. W. C. Chan, M. N. O'Sullivan, and R. W. Boyd, Optimization of thermal ghost imaging: High-order correlations vs. background subtraction, Opt. Express 18, 5562 (2010).

[8] R. E. Meyers, K. S. Deacon, and Y. Shih, Positive-negative turbulence-free ghost imaging, Appl. Phys. Lett. 100, 131114 (2012).

[9] M. Bina, D. Magatti, M. Molteni, A. Gatti, L. A. Lugiato, and F. Ferri, Backscattering Differential Ghost Imaging in Turbid Media, Phys. Rev. Lett. 110, 083901 (2013).

[10] X.-F. Liu, X.-H. Chen, X.-R. Yao, W.-K. Yu, G.-J. Zhai, and L.-A. Wu, Lensless ghost imaging with sunlight, Opt. Lett. 39, 2314 (2014).

[11] M. G. Capeluto, H. Duisterwinkel, C. T. Schmiegelow, D. Francisco, S. Ledesma, and C. Iemmi, Ghost imaging and ghost diffraction with pseudo-thermal light generated by means of a programmable SLM, J. Phys. Conf. Ser. 274, 012004 (2011).

[12] S. Hartmann and W. Elsäßer, A novel semiconductor-based, fully incoherent amplified spontaneous emission light source for ghost imaging, Sci. Rep. 7, 41866 (2017).

[13] Y. Bromberg, O. Katz, and Y. Silberberg, Ghost imaging with a single detector, Phys. Rev. A 79, 053840 (2009).

[14] S. Hartmann, A. Molitor, and W. Elsäßer, Ultrabroadband ghost imaging exploiting optoelectronic amplified spontaneous emission and two-photon detection, Opt. Lett. 40, 5770 (2015).

[15] S. Kuhn, S. Hartmann, and W. Elsäßer, Photon-statistics-based classical ghost imaging with one single detector, Opt. Lett. 41, 2863 (2016).

[16] R. E. Meyers, K. S. Deacon, and Y. Shih, Turbulence-free ghost imaging, Appl. Phys. Lett. 98, 111115 (2011).

[17] P. Clemente, V. Durán, V. Torres-Company, E. Tajahuerce, and J. Lancis, Optical encryption based on computational ghost imaging, Opt. Lett. 35, 2391 (2010).

[18] L. A. Lugiato, "Ghost imaging": Fundamental and applicative aspects, Rend. Inst. Lomb. Accad. Sci. Lett. 147, 139 (2013).

[19] R. S. Aspden, N. R. Gemmell, P. A. Morris, D. S. Tasca, L. Mertens, M. G. Tanner, R. A. Kirkwood, A. Ruggeri, A. Tosi, R. W. Boyd, G. S. Buller, R. H. Hadfield, and M. J. Padgett, Photon-sparse microscopy: Visible light imaging using infrared illumination, Optica 2, 1049 (2015).

[20] D. Pelliccia, A. Rack, M. Scheel, V. Cantelli, and D. M. Paganin, Experimental X-Ray Ghost Imaging, Phys. Rev. Lett. 117, 113902 (2016).

[21] R. I. Khakimov, B. M. Henson, D. K. Shin, S. S. Hodgman, R. G. Dall, K. G. H. Baldwin, and A. G. Truscott, Ghost imaging with atoms, Nature (London) 540, 100 (2017).

[22] F. Devaux, K. P. Huy, S. Denis, E. Lantz, and P.-A. Moreau, Temporal ghost imaging with pseudo-thermal speckle light, J. Opt. 19, 024001 (2017).

[23] P. Ryczkowski, M. Barbier, A. T. Friberg, J. M. Dudley, and G. Genty, Ghost imaging in the time domain, Nat. Photonics 10, 167 (2016).

[24] F. Devaux, P.-A. Moreau, S. Denis, and E. Lantz, Computational temporal ghost imaging, Optica **3**, 698 (2016).

[25] G. Scarcelli, A. Valencia, S. Gompers, and Y. Shih, Remote spectral measurement using entangled photons, Appl. Phys. Lett. **83**, 5560 (2003).

[26] J. Strong, National Technical Information Service, Cambridge Research Laboratories Report No. AFCRL-72-0085, 1972.

[27] N. J. Sloane, Multiplexing methods in spectroscopy, Math. Mag. **52**, 71 (1979).

[28] S. Denis, P.-A. Moreau, F. Devaux, and E. Lantz, Temporal ghost imaging with twin photons, J. Opt. **19**, 034002 (2017).

[29] D. I. Kalashnikov, A. V. Paterova, S. P. Kulik, and L. A. Krivitsky, Infrared spectroscopy with visible light, Nat. Photon. **10**, 98 (2016).

[30] B. Sun, M. P. Edgar, R. Bowman, L. E. Vittert, S. Welsh, A. Bowman, and M. J. Padgett, 3D computational imaging with single-pixel detectors, Science **340**, 844 (2013).

[31] F. Boitier, A. Godard, E. Rosencher, and C. Fabre, Measuring photon bunching at ultrashort timescale by two-photon-absorption in semiconductors, Nat. Phys. **5**, 267 (2009).

[32] M. Grundmann, *Nano-Optoelectronics: Concepts, Physics and Devices* (Springer, Berlin, 2002), Chap. 10, pp. 239–272.

[33] T. Iskhakov, A. Allevi, D. A. Kalashnikov, V. G. Sala, M. Takeuchi, M. Bondani, and M. Chekhova, Intensity correlations of thermal light—Noise reduction measurements and new ghost imaging protocols, Eur. Phys. J. Spec. Top. **199**, 127 (2011).

[34] A. Gatti, M. Bache, D. Magatti, E. Brambilla, F. Ferri, and L. A. Lugiato, Coherent imaging with pseudo-thermal incoherent light, J. Mod. Opt. **53**, 739 (2006).

[35] S. Hartmann, S. Kuhn, and W. Elsäßer, Characteristic properties of the spatial correlations and visibility in mixed light ghost imaging, Appl. Opt. **55**, 7972 (2016).

[36] S. Kedenburg, M. Vieweg, T. Gissibl, and H. Giessen, Linear refractive index and absorption measurements of nonlinear optical liquids in the visible and near-infrared spectral region, Opt. Mater. Express **2**, 1588 (2012).